

HYDROFOILS WITH DIFFERING LEADING-EDGE PROTUBERANCES: CFD AND EXPERIMENTAL INVESTIGATIONS

(Reference No: IJME673, DOI No: 10.5750/ijme.v163iA3.799)

R. Kant and A. Bhattacharyya, Indian Institute of Technology Kharagpur, West Bengal, India

KEY DATES: Submitted: 14/09/20; Final acceptance: 17/05/21; Published 16/11/21

SUMMARY

Leading-edge protuberances on the pectoral fin of humpback whales have been widely adopted to the designs of foils to provide superior lifting characteristics in the post-stall regimes. The present work investigates the lift, drag and flow characteristics of finite-span rectangular hydrofoils having different configurations of two protuberances over the leading edge with NACA 63₄-021 as the base design section. The results obtained from CFD analyses are validated using lift and drag measurements from experiments. The influence of using a transition-sensitive turbulence model on the results is investigated. It is observed that, in general, a foil with smaller separation between protuberances has better post-stall lift characteristics whereas that with protuberances at larger separation have better pre-stall characteristics. Depending on the separation between them, streamwise vortices are generated from the leading-edge protuberances. The two protuberances can restrict the zone of separation between them at high angles of attack. The influence of Reynolds number on the lifting performance is also investigated.

NOMENCLATURE

A	Amplitude of protuberance (m)
c	Chord Length (m)
C_D	Drag Coefficient
C_L	Lift Coefficient
D	Drag Force (N)
L	Lift Force (N)
n	Number of tubercles
Re	Reynold's number with respect to the chord
S	Span (m)
U_∞	Freestream Velocity (m/s)
x	x-coordinate
z	z-coordinate
α	Angle of attack (deg)
λ	Wavelength of protuberance (m)
ν	Dynamic viscosity ($\text{kg m}^{-1} \text{s}^{-1}$)
ρ	Density(kg/m^3)

2004) showing a 40% delay in the stall angle with an increase in post-stall lift.

A numerical study performed by (Cai et al., 2015) over NACA 63₄-021 baseline foil and other two modified foils with leading-edge protuberances having different amplitudes reported an increase in post-stall lift. The modified foil with smaller amplitude of protuberance performs similar to the baseline foil, while lift increases in the post-stall region for the modified foil with higher amplitude protuberances. A number of studies have been done on the effect of protuberance amplitude over lift characteristics. An experimental study for airfoils with uniformly distributed tubercles of different amplitudes and wavelengths was presented by (Johari et al., 2007), which suggested that wavelengths of the protuberances play a minor role in the lift enhancement, while amplitude had a more significant effect. A similar effect has been found from many other numerical (Cai et al., 2015) and experimental (Chen et al., 2012; Wei et al., 2019) works. Experimental evidence has also been gathered to explain the phenomenon including the presence of wall-normal (transverse) vorticity in the flow at low $Re = 800$ (Favier et al., 2012). Numerical investigations have attributed it to a secondary flow mechanism that enhances momentum transfer and reduces flow separation in the transitional flow regime (Skillen et al., 2015); reorganization of spanwise vorticity into streamwise and transverse vorticity (Rostamzadeh et al., 2017); induced downwash effect over tubercle peaks and upwash on tubercle troughs (Van Nierop et al., 2008).

1. INTRODUCTION

The humpback whales are the most agile among their species. Their excellent maneuverability has been attributed to the tubercles over the leading edge of their flippers (Fish and Battle, 1995). These tubercles are hump-like modifications or protuberances which alter the flow hydrodynamics around the whale flippers and work as lift enhancement devices (Fish and Lauder, 2006; Miklosovic et al., 2004). They help the flow to remain attached up to a larger angle of attacks thus increasing the stall angle (Fish et al., 2011).

Several research works have been done investigating the effects of tubercles over the leading edge of foil using numerical and experimental methods. A wind tunnel experiment was done by (Miklosovic et al.,

Considering the available literature on leading-edge modified foils presented till now, the modifications were restricted to uniformly distributed humps/protuberances over the span of the foil. However, in some published works, the distribution of leading-edge protuberance is not uniform. A numerical

study was performed by (Arai et al., 2010) having protuberances on the leading edge separated at a distance and found that it is as effective as that of continuous protuberances. A numerical and experimental study done by (Cai et al., 2018) on an airfoil having a single leading-edge protuberance showed that it can generate streamwise vortices like continuous protuberances. An experimental and numerical study performed by (Srinivas et al., 2018) over a rudder had found that the leading-edge tubercle design similar to that of a humpback whale is able to restrict the flow separation between two large protuberances which led to better post-stall lift characteristics as compared to continuous protuberances.

In the present study, the two prominent protuberances mimicked from the first and fourth tubercles of the humpback whale flipper are added over the leading edge of a hydrofoil to obtain better post-stall lift. However, a symmetric hydrofoil design about the mid-span is chosen, and the distance between the protuberances is varied to understand the influence on the flow patterns and lift-drag characteristics at different angles of attack.

2. GEOMETRY

A symmetrical hydrofoil (NACA 63₄-021) is taken as the baseline design having span ($s = 200$ mm) and chord length ($c = 100$ mm). The protuberances over the leading edge are defined geometrically using equation (1).

$$\Delta c = \bar{A} \sin \left[2\pi \left(\frac{z - z_i}{\lambda} \right) \right] \quad \forall \quad z_i \leq z \leq z_f \quad (1)$$

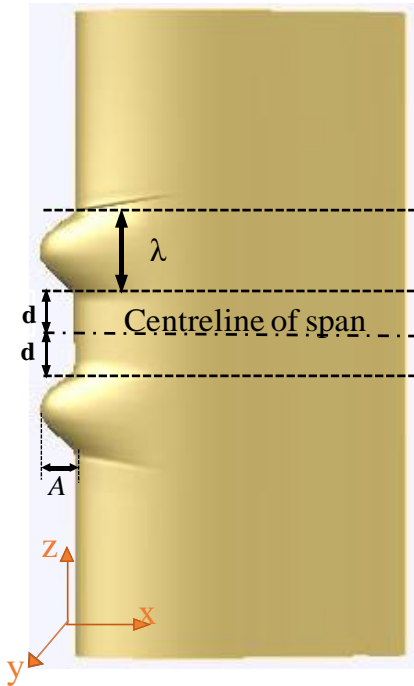


Figure 1: Geometry of the hydrofoil with two leading edge protuberances
The design of a leading-edge protuberance is shown in Figure 1. \bar{A} and λ are the amplitude and wavelength of the

protuberances. z_i and z_f are the initial and final z coordinates respectively of the protuberances over the leading edge.

A positioning study is performed in this work for the twin protuberances considering six cases: $d = 0, 5, 10, 15, 20$ and 30 percent of span, where d is the distance of the protuberance base from the centerline of the span as shown in Figure 1.

3. INVESTIGATIONS

A comparative analysis of the lift and drag coefficients and flow characteristics for the different hydrofoil designs is done using CFD analyses. A validation study is performed for a modified foil with two leading edge protuberances using measurements of lift and drag from experiments.

3.1 CFD ANALYSES

The Reynolds-averaged Navier-Stokes (RANS) solver of STAR CCM+ is used with the SST $k-\omega$ turbulence model because it performs better for flows with adverse pressure gradient (Menter et al., 2003). The governing equations used for CFD simulations are as follows.

$$\frac{\partial U_i}{\partial x_i} = 0 \quad (2)$$

$$\rho \frac{\partial k}{\partial t} + \rho U_j \frac{\partial k}{\partial x_j} = \tau_{ij} \frac{\partial U_i}{\partial x_j} - \beta^* \rho k \omega + \frac{\partial}{\partial x_j} \left[(\mu + \sigma^* \mu_T) \frac{\partial k}{\partial x_j} \right] \quad (3)$$

$$\rho \frac{\partial \omega}{\partial t} + \rho U_j \frac{\partial \omega}{\partial x_j} = \alpha \frac{\omega}{k} \tau_{ij} \frac{\partial U_i}{\partial x_j} - \beta^* \rho \omega^2 + \frac{\partial}{\partial x_j} \left[(\mu + \sigma \mu_T) \frac{\partial \omega}{\partial x_j} \right] \quad (4)$$

In the above equations U_i represents the flow velocity in i -direction, ρ -the density, k - turbulence kinetic energy, ω -the rate of dissipation of the turbulence kinetic energy and μ - the dynamic viscosity of the fluid.

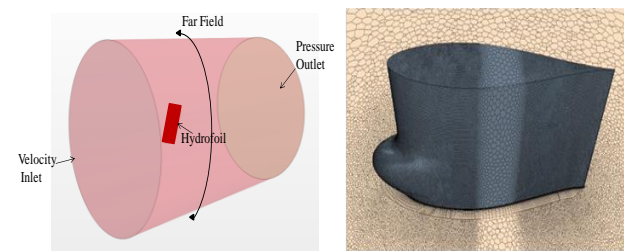


Figure 2: Computational domain and mesh.

As shown in Figure 2, a cylindrical computational domain is used having polyhedral cells over the domain and prism layers on the hydrofoil boundary for capturing the boundary layer flow and separation. The inlet and outlet boundary are set at distance of $5c$ and $13c$, and the far-field radius is set at $5c$. To capture the velocity gradients two volumetric cylinders are placed

at the leading and trailing edges of the hydrofoil for local grid refinement. The total grid size of the computational domain is around 2 million. The wall y^+ value close to 1 is maintained near the foil boundary. A grid dependency study is performed at 15° angle of attack, where it has been found that the C_L and C_D converge satisfactorily for the chosen grid resolution.

3.2 EXPERIMENTS

Measurements of lift and drag forces are conducted in the towing tank of the Department of Ocean Engineering and Naval Architecture at IIT Kharagpur. The foil is connected to the towing carriage using a structural mount (Figure 3). The structural mount is equipped with an encoder, a stepper motor, and a load cell. The stepper motor is used to rotate the hydrofoil, and it is attached with an encoder which gives feedback of the actual angle turned. To avoid free surface effect the top surface of the hydrofoil is immersed at a depth of $1.5c$ from the free surface. The diameter of connecting rod is 8 mm and it is kept at 0.25 of chord length, therefore tip vortices doesn't get effected much by connecting rod. Force measurements averaged over 20 sec are obtained using data acquisition system. The required flow velocity of 2 m/s is obtained by moving the hydrofoil connected to the structural mount and carriage on rails installed along the length of the tank.

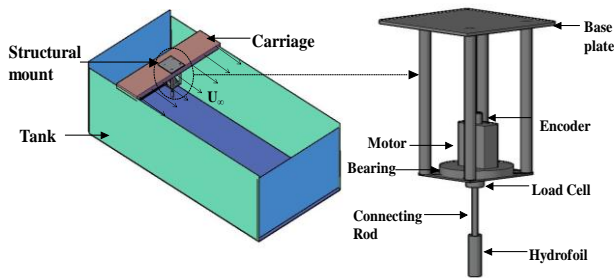


Figure 3: Foil with structural mount and measurement system attached to the carriage on the towing tank.

An assessment of precision uncertainty of the experimental results is performed by taking five repeated measurements of drag and lift values at $\alpha = 15$ deg. The calculated uncertainties using Students't' distribution at 95% confidence interval are less than 2% for both drag and lift coefficients.

4. VALIDATION STUDY

The CFD results were validated using experimental measurements of lift and drag coefficients at $Re = 2 \times 10^5$. Figure 4 shows that experimental results at different angles of attack are in good agreement with CFD results. The calculated lift coefficient in post stall angles is slightly higher than the experimental results which may be due to the limitation of RANS model for largely separated flows (Menter et al., 2003). The differences may also arise due

to the interaction of the hydrofoil tip vortices with the free surface in the experiments at higher angles of attack.

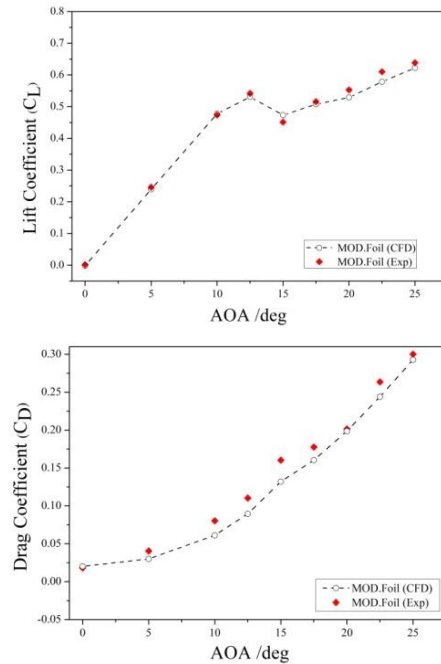


Figure 4: Lift and Drag coefficients for the hydrofoil with two protuberances (Experiments and CFD).

A verification of the CFD results has been performed following the methods presented in (Stern et al. 1999), where the uncertainty due to grid size is calculated using generalized Richardson extrapolation. Three different successively refined grids are generated using a grid refinement factor of $\sqrt{2}$. The force coefficients for the different grids- (coarse (u_h) = 0.7 million, medium (u_{rh}) = 2 million, fine (u_{r2h}) = 4 million) are used for the convergence study. The convergence ratio (R) as defined in eq. 5 is calculated for the lift coefficient.

$$R = \frac{u_{r2h} - u_{rh}}{u_{rh} - u_h} \quad (5)$$

For the present case, R is less than 1, indicating mesh convergence in the fluid domain. The error of the fine grid (ϵ_h), order of accuracy (\hat{p}) and correction factor (C_G) are calculated as 0.41% of u_{r2h} , 3.53 and 2.398 respectively. The grid uncertainty (U_G), estimated error of the fine grid (ϵ_h), and correction solution (U) are evaluated as:

$$U_G = (2|1 - C_G| + 1)\epsilon_h(p) \approx 0.327\% \text{ of } u_{r2h}$$

$$\epsilon_h = C_G \bar{\epsilon}_h(p) \approx 5.995 \times 10^{-3} = 0.59\% \text{ of } u_{r2h}$$

Since, $U=0.611$, the generalized Richardson extrapolation can be used to estimate the uncertainty for the medium grid solution as 0.5% of u_{rh} which is acceptable. Further, due to lower computational time and reasonably good agreement with the experimental results, the same has been used for the entire numerical study.

5. RESULTS AND DISCUSSIONS

The lift and drag coefficients of the six hydrofoil designs with two protuberances at varied spacing are compared with the base NACA 634-021 foil using CFD analyses. Comparative flow analyses at different angles of attack are presented to understand the underlying flow physics involved for the different configurations.

5.1 EFFECT OF PROTUBERANCE SPACING

The lift, drag, and flow characteristics like velocity, vortices and pressure distribution of the foils at $Re = 2 \times 10^5$ are presented in this section. The C_L , C_D and C_L/C_D comparison at different angles of attack are shown in Figure 5. The lift coefficient of all the modified foils are found to be very similar to that of the base foil until $\alpha = 10$ deg. After $\alpha \geq 10$ deg, the lift for all modified foils is lower than the base foil which has a much higher maximum lift coefficient. However, in the post-stall regime ($\alpha > 20$ deg) all the modified foils provide higher lift than that of the base foil except for the foil with the highest spaced protuberances ($d= 30\%$ of s). The foil designs with protuberances show much milder stall characteristics compared to the unmodified base foil.

For the modified foil designs, the lift coefficient is found to increase as d increases in the pre-stall region. In the post-stall region, the lift coefficient is maximum when d is minimum. Also, all the foils have similar drag coefficients till $\alpha = 10$ deg, after which the values differ depending on the angle of attack. From the C_L/C_D curve it can be seen that closer protuberance performs better in the post-stall region, while foils with protuberances at larger distance perform better in the pre-stall region.

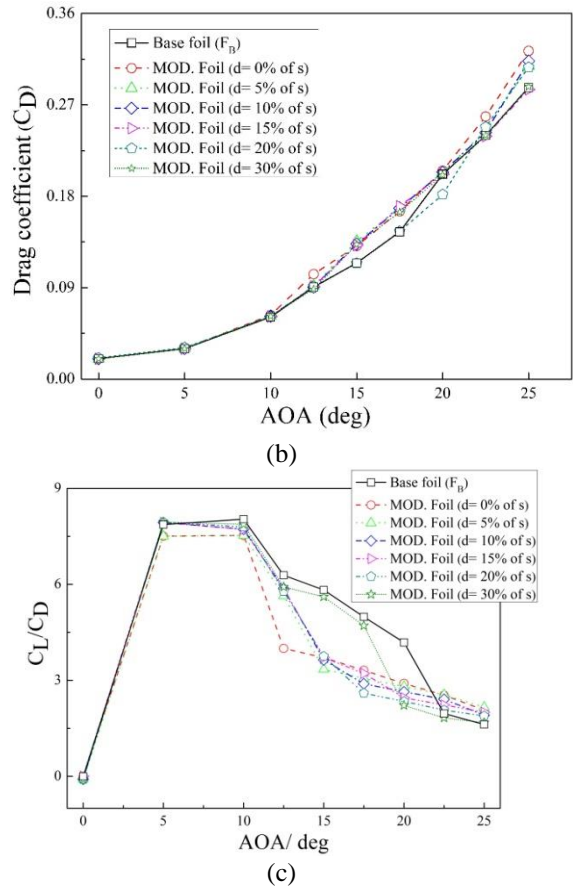
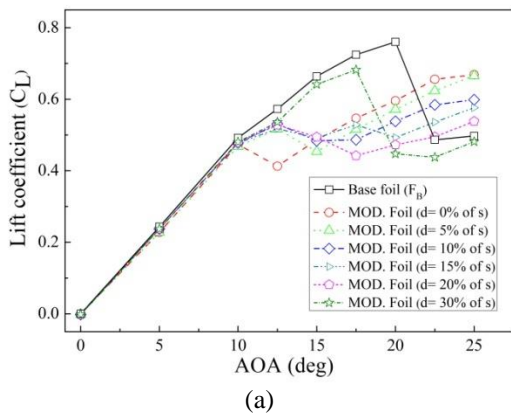


Figure 5: (a) Lift coefficient and (b) Drag coefficient (c) Lift/Drag ratio for foils with two protuberances having different positions (CFD results).

The lift and drag characteristics are mainly dependent on the surface flow patterns which govern the pressure distribution and stall angles for the individual designs. Considering the foils with protuberances, the increase in lift characteristics compared to the base foil is restricted to the high angles of attack ($\alpha \geq 22.5$ deg), which is in the post-stall regime of the base foil. Therefore, a detailed flow analysis involving vorticity, pressure distribution and velocity contours is presented at $\alpha = 25$ deg to understand the relative performance of all the foil designs.

It is well established that leading edge protuberances can help in generating streamwise vortices on airfoils. The modified foils in the present study show distinct vorticity development from the two protuberances at the leading edge, which is not observed in the base foil. These vortices re-energize the boundary layer by transferring the momentum due to which the flow separation over the modified foils is reduced at high angles of attack.

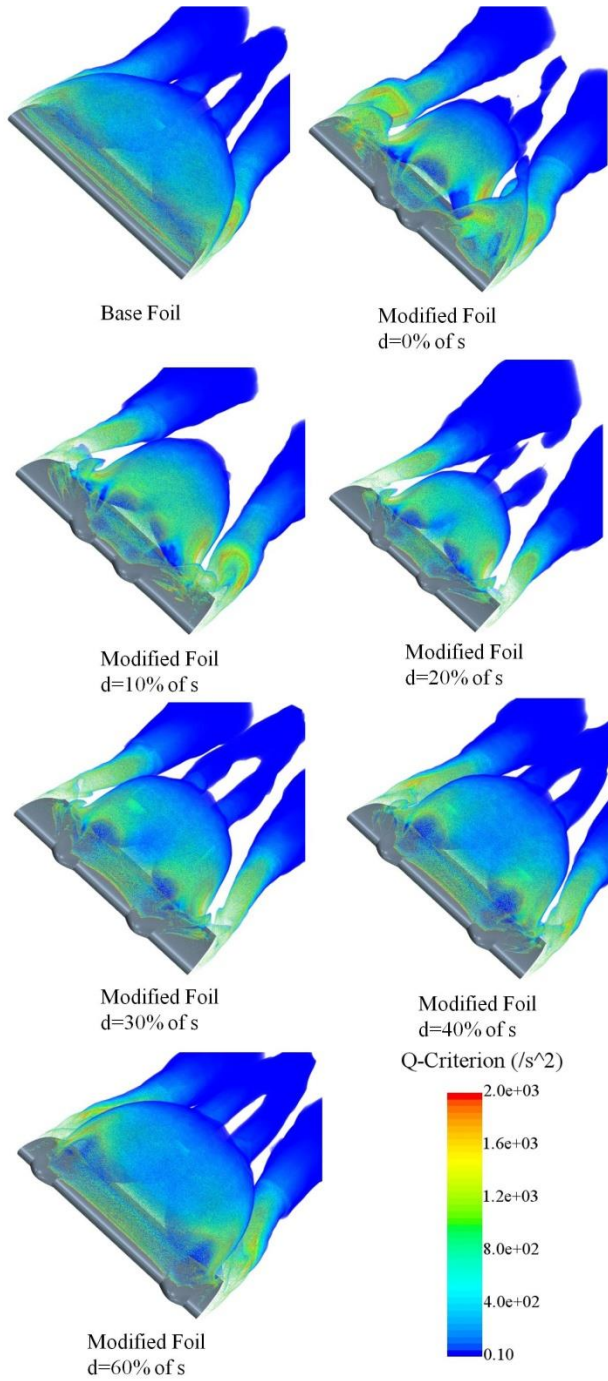


Figure 6: Plots of positive Q-criterion over a resampled volume around the hydrofoil designs at $\alpha = 25$ deg to show dominance of rotation rate tensor.

In the present study, the Q-criterion is used for vortex visualisation over the hydrofoil designs.

The Q-criterion is directly derived from the velocity gradient tensor $\frac{\delta u_i}{\delta x_j}$ which can be broken into two parts such that

$$\frac{\delta u_i}{\delta x_j} = S + \Omega \quad (6)$$

Here 'S' is the symmetrical part of velocity gradient tensor known as strain rate tensor defined as-

$$S = 1/2 \left[\left(\frac{\delta u_i}{\delta x_j} \right) + \left(\frac{\delta u_j}{\delta x_i} \right) \right] \quad (7)$$

The antisymmetric part denoted as Ω is known as the rotation rate or vorticity tensor defined by-

$$\Omega = 1/2 \left[\left(\frac{\delta u_i}{\delta x_j} \right) - \left(\frac{\delta u_j}{\delta x_i} \right) \right] \quad (8)$$

However, Q is defined as the second invariant of the velocity gradient tensor.

$$Q = 1/2 \left(|\Omega|^2 - |S|^2 \right) \quad (9)$$

The positive value of Q indicates a flow field dominated by vorticity, while a negative value indicates the dominance of strain rate or viscous stress. In the present case, the positive value of Q is shown in Figure 6 to understand the vorticity development over the suction surface of the hydrofoils. For the modified designs, two symmetric vortical zones are formed due to the chordwise vortices shed downstream from the two protuberances. The zone between them has higher viscous stress and hence Q is negative in that domain. The chordwise vortices gradually diffuse downstream of the trailing edge. Also, strong tip vortices are observed from all the hydrofoils, which merge with the streamwise vortices from the protuberances for the design with maximum spacing.

For the modified foils, the streamlines on either side of the protuberances converge causing a streamwise vorticity, which is stronger for closely spaced protuberances. These vortices result in low pressure on the suction surface of modified foils which cause lift enhancement in the post-stall regime. The pressure contours over the foil surface at $\alpha = 25$ deg is shown in Figure 7. The lower pressure on the surface of modified foils leads to an increase in lift up to 20%. For modified foils, the low-pressure zones are created from both ends of span to the trough of the respective protuberances which results in flow attachment in that region. Therefore, as the distance between the protuberances increases, the extent of low-pressure zone decreases because of which lift decreases in the post-stall. This is evident from the similarity of the lift coefficient curve between the base foil and the design with largest spaced protuberances ($d= 30\%$ of s). On the other hand, for the smallest spacing case ($d= 0\%$ of s), the low-pressure zone starts to get weaker towards both the ends of the span. For all the modified foils, a favourable pressure gradient is generated from the troughs of the protuberances towards the trailing edge causing flow attachment at high angles of attack.

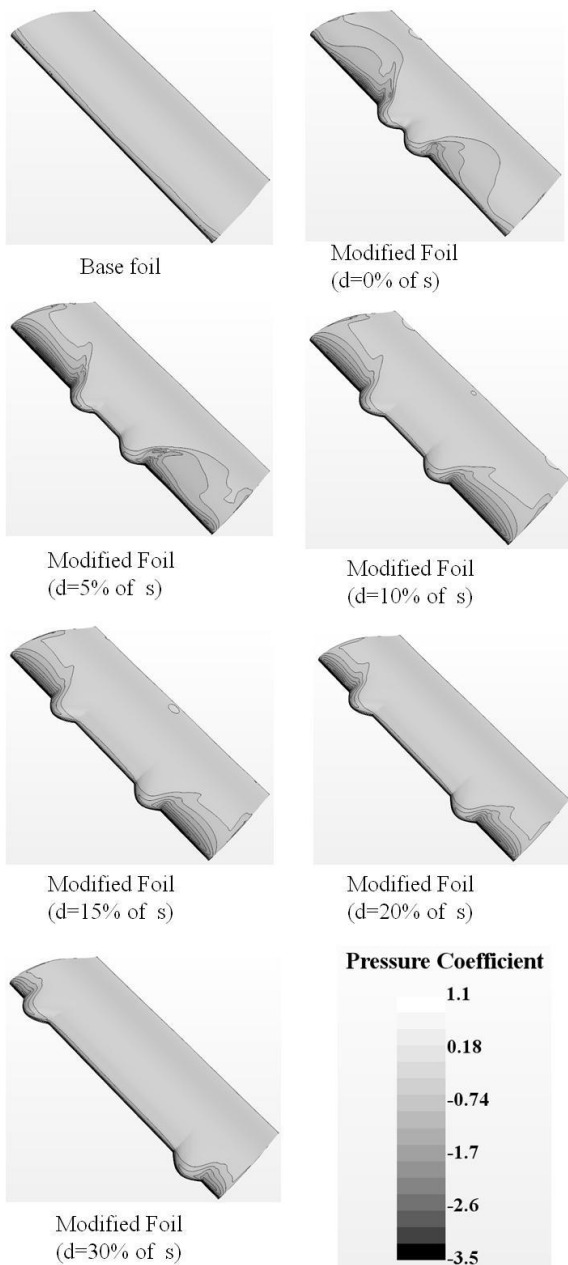


Figure 7: Pressure coefficient over the base foil and modified foil designs at $\alpha = 25$ deg

The modified foils can also restrict the separation zone due to the streamwise vortices generated from the protuberances as shown in Figure 8, where a volumetric plot of the reversed velocity indicating flow separation and re-circulation over the suction surface side at the high angle of attack, $\alpha = 25$ deg. Especially for the designs with intermediate protuberance spacings with respect to $d = 5, 10$ and 15% of s , the chordwise vortices from the two protuberances interact strongly at this angle resulting in greater control of the post-stall separation domain. This is a characteristic feature for the foil with two leading edge protuberances which is proposed in this work, as a simplified bio-mimicry of the humpback whale flipper.

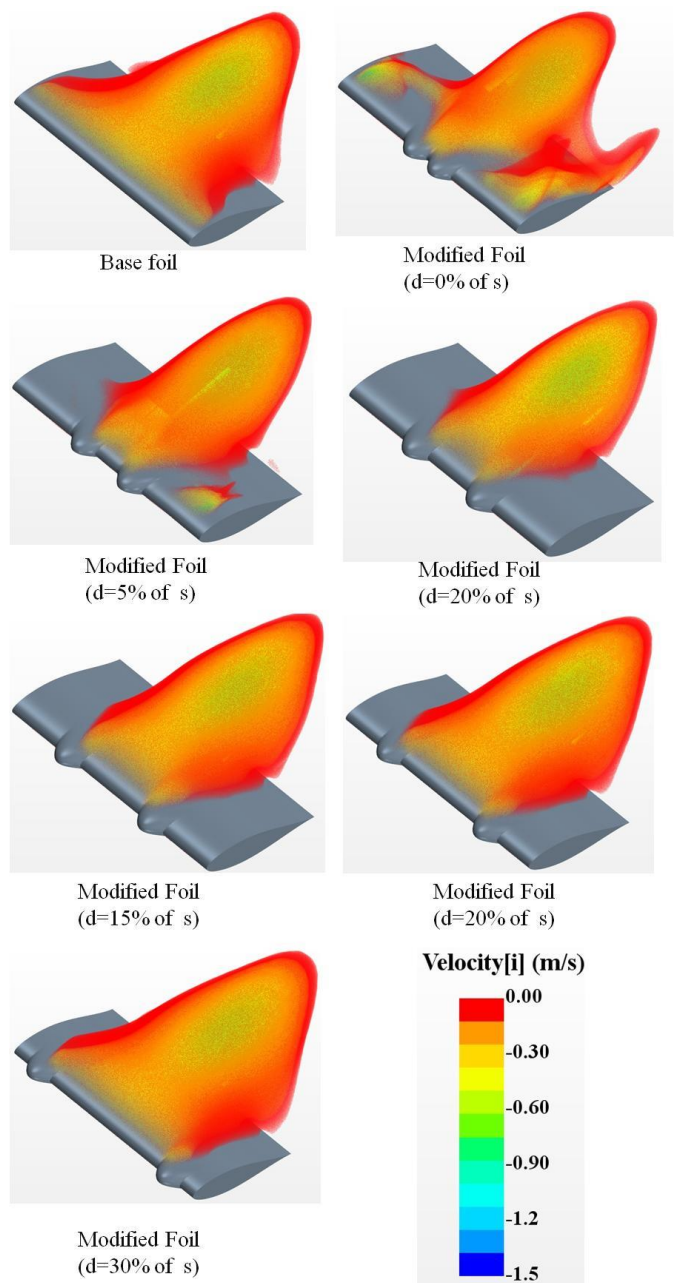


Figure 8: Plots of reversed velocity contours indicating flow separation and re-circulation over the hydrofoils at $\alpha = 25$ deg

5.2 INVESTIGATIONS USING TRANSITION MODEL IN CFD

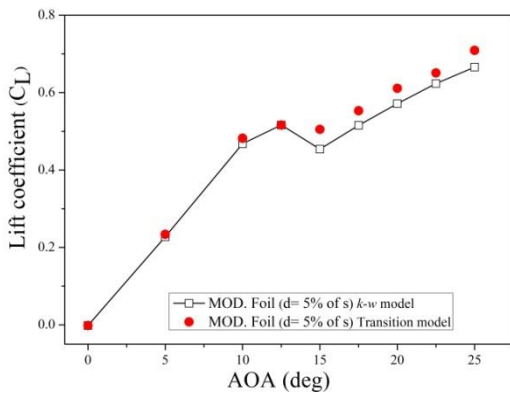
The Reynolds number corresponding to the investigations is 2×10^5 for which transitional flow regimes may exist over certain zones over the foil designs. Hence, CFD calculations were also done using the γ - Re_{θ} transition model and a comparison of the foil forces are presented with the results using the $k-\omega$ SST turbulence model.

The used transition model is a correlation-based model in which the value of intermittency (γ) depends on the transition momentum thickness Reynolds number ($Re_{\theta t}$) through a correlation defined in the free stream. The variable $Re_{\theta t}$ is defined by a value of wall distance which is used to transport the free stream value to the boundary

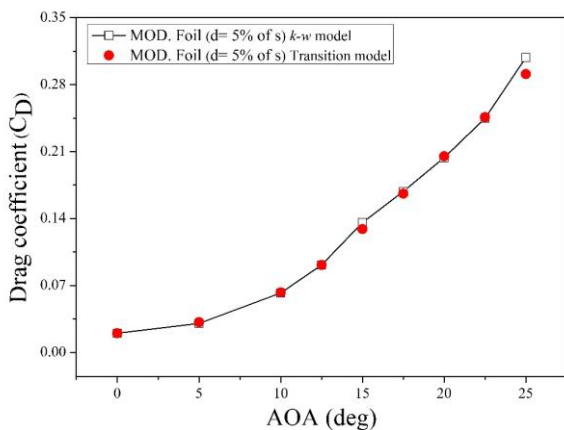
layer. The turbulence viscosity ratio plays a vital role in the transition model study- a smaller value leads to higher turbulence decay, while a higher value causes excessive diffusion. It is observed that the inlet turbulence intensity reduces to 50% when it reaches the leading edge of the foil. To avoid this turbulent kinetic energy sources are used in the fluid domain as mentioned flow separation over the suction surface of the foils in (Bhattacharyya et al., 2015). The turbulence kinetic energy source term is specified as in equation (10).

$$k_{source} = \frac{3}{2} \times \left(TI_{required}^2 - TI_{existing}^2 \right) \times U_{\infty}^2 \quad (10)$$

Here, k_{source} is the turbulence source strength, U_{∞} is the flow velocity at the inlet, $TI_{required}$ is the turbulence intensity required, and $TI_{existing}$ is the turbulence intensity existing in the domain. The source term helps to maintain the turbulence intensity in the domain of interest, which can later be terminated by a switch function in front of the foil to avoid additional turbulence in the boundary layer.



(a)

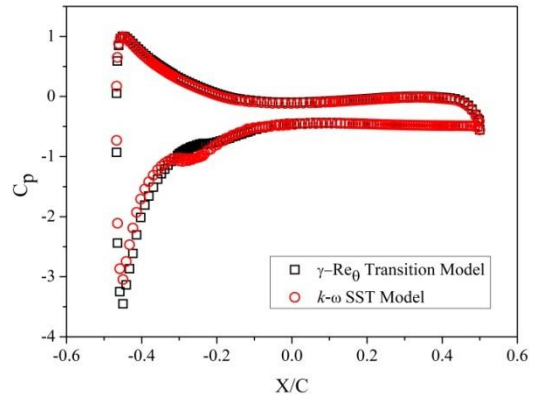


(b)

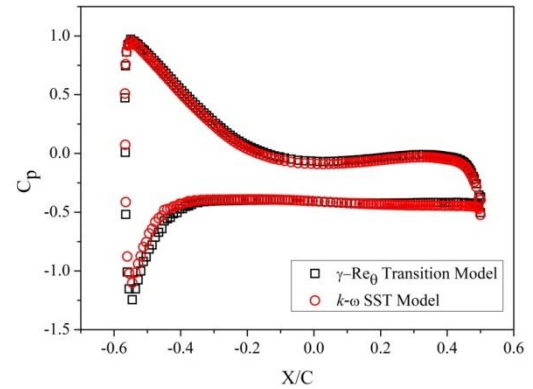
Figure 9: (a) Lift coefficient and (b) Drag coefficient for a foil with protuberances (d = 5% of c): Comparison of results using turbulence and transition models in CFD

The comparison plot of force coefficients using transition and standard turbulence models for a modified foil (d= 5% of s) is shown in Figure 9. In general, the lift and drag coefficients are very similar between the two models.

However, at angles of attack higher than 12.5 deg, higher lift coefficients are predicted using the transition model. To investigate this outcome, the chordwise pressure distributions at $\alpha = 25^\circ$ over the crest and trough of the modified foil obtained using the $k-\omega$ SST model and the $\gamma-Re_\theta$ transition model are compared in Figure 10.



(a)



(b)

Figure 10: Pressure coefficients over two sections for $\alpha=25^\circ$ of the modified foil (d= 5% of s): (a) trough, and (b) crest

In Figure 10, $x/c = -0.5$ denotes the leading edge and $x/c = 0.5$ denotes the trailing edge of the foils. The pressure coefficient is given by equation 11.

$$C_p = \frac{p - p_{\infty}}{\frac{1}{2} \rho_{\infty} V_{\infty}^2} \quad (11)$$

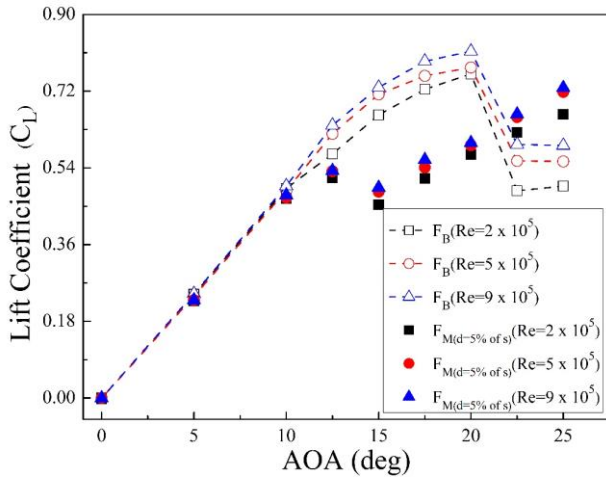
Where C_p , p , p_{∞} , ρ_{∞} and V_{∞} are the pressure coefficient, static pressure on the hydrofoil, stagnation pressure in the far-field, free-stream fluid density and far-field velocity of the fluid respectively.

For the modified foil with two protuberances, it is observed that the peak suction pressure amplitude is considerably higher along the trough as compared to the crest section. The negative pressure coefficient near the leading edge obtained using the transition model is higher than that using the $k-\omega$ SST model. As the flow becomes turbulent towards the trailing edge, the two models predict similar pressure

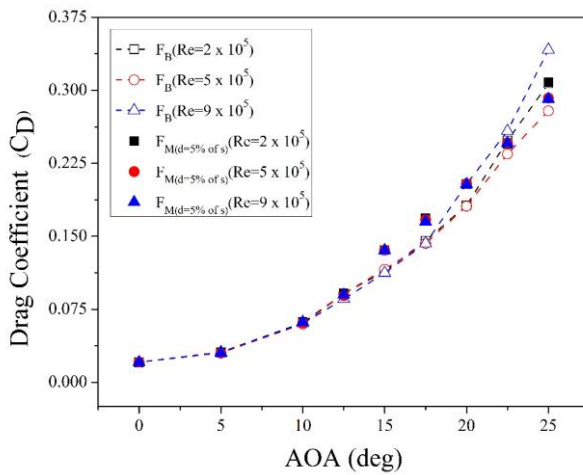
values. Since the pressure difference between the two surfaces of the foil is higher near the leading edge, a greater lift coefficient is obtained using the transition model at high angles of attack.

5.3 REYNOLDS NUMBER EFFECT ON FOIL COEFFICIENTS

The comparison of lift and drag coefficients at three different Reynolds numbers (2×10^5 , 5×10^5 and 9×10^5) for the base foil (F_B) and the modified foil ($F_{M(d=5\% \text{ of } s)}$) is shown in Figure 11.



(a)



(b)

Figure 11: (a) Lift coefficient, and (b) Drag coefficient for the base foil and a modified foil at three Reynolds numbers

The lift coefficient is found to increase significantly for both the foils for $\alpha \geq 10^\circ$, especially at $Re = 9 \times 10^5$. The stall characteristics are however very much similar for all the Reynolds numbers. The drag coefficient does not change much for modified foil but for base foil it increases with Reynolds number at high angles of attack. For all the

cases, the base foil has a considerably higher maximum lift coefficient, and the modified foil provides better post-stall lift at $\alpha \geq 22.5^\circ$.

6. CONCLUSIONS

The lift and drag characteristics of a hydrofoil having NACA 634-021 section and aspect ratio of 2 with two protuberances over the leading edge are investigated. The chordwise vortices generated by each protuberance interact to reduce the flow separation at high angles of attack, depending on the separation between them. The modified foils have lower maximum lift coefficient and higher lift in the post-stall region compared to the base foil. The pre-stall and post-stall lift characteristics can be altered by suitably designing the separation between the protuberances. In the selected range of Reynolds number ($2 \times 10^5 \geq Re \leq 9 \times 10^5$), the increase of post-stall lift coefficient for the hydrofoil with two protuberances is in the range of 14-39% of that of the unmodified base design with NACA 634-021 profile. The modified foil with two leading edge protuberances can hence be suitably tailored for high angle of attack applications.

7. ACKNOWLEDGMENTS

The funding support received from Science and Engineering Research Board, Government of India through Project No. ECR/2018/000565 is acknowledged.

8. REFERENCES

1. ARAI, H., DOI, Y., NAKASHIMA, T., and MUTSUDA, H. (2010) 'A Study on Stall Delay by Various Wavy Leading Edges', Journal of aero aqua bio-mechanisms, 1(1), pp. 18–23.
2. BHATTACHARYYA, A., NEITZEL, J., STEEN, S., ABDEL-MAKSOU, M., and KRASILNIKOV, V. (2015) 'Influence of flow transition on open and ducted propeller characteristics', in Fourth International Symposium on Marine Propulsors, Austin, Texas, USA.
3. CAI, C., ZUO, Z., LIU, S., and WU, Y. (2015) 'Numerical investigations of hydrodynamic performance of hydrofoils with leading-edge protuberances', Advances in Mechanical Engineering, 7(7), pp. 1-11.
4. CAI, C., ZUO, Z., LIU, S., and MAEDA, T. (2018) 'Effect of a single leading-edge protuberance on NACA 634-021 airfoil performance', Journal of Fluids Engineering, 140(2), pp. 1-7.
5. CHEN, J. H., LI, S. S. and NGUYEN, V. T. (2012) 'The effect of leading edge protuberances on the performance of small aspect ratio foils', in 15th International Symposium of Flow Visualization

- ISFV15-040-S21, Minsk, Belarus, pp.1-16.
6. FAVIER, J., PINELLI, A. and PIOMELLI, U. (2012) 'Control of the separated flow around an airfoil using a wavy leading edge inspired by humpback whale flippers', *Comptes Rendus Mecanique*, 340(1-2), pp. 107-114.
 7. FISH, F. E., WEBER, P. W., MURRAY, M. M., and HOWLE, L.E. (2011) 'Marine applications of the biomimetic Humpback whale flipper', *Marine Technology Society Journal*, 45(4), pp. 198-207.
 8. FISH, F. E. and BATTLE, J. M. (1995) 'Hydrodynamic design of the humpback whale flipper', *Journal of Morphology*, 225(1), pp. 51-60.
 9. FISH, F. E. and LAUDER, G. V (2006) 'Passive and active flow control by swimming fishes and mammals', *Annu. Rev. Fluid Mech*, 38, pp. 193-224.
 10. JOHARI, H., HENOCH, C. W., CUSTODIO, D., and LEVSHIN, A. (2007) 'Effects of leading-edge protuberances on airfoil performance', *AIAA Journal*, 45(11), pp. 2634-2642.
 11. MENTER, F. R., KUNTZ, M. and LANGTRY, R. (2003) 'Ten years of industrial experience with the SST turbulence model', *Turbulence, heat and mass transfer*, 4(1), pp. 625-632.
 12. MIKLOSOVIC, D. S., MURRAY, M. M., HOWLE, L. E., and FISH, F. E., (2004) 'Leading-edge tubercles delay stall on humpback whale (*Megaptera novaeangliae*) flippers', *Physics of fluids*, 16(5), pp. L39-L42.
 13. VAN NIEROP, E. A., ALBEN, S. and BRENNER, M. P. (2008) 'How bumps on whale flippers delay stall: an aerodynamic model', *Physical review letters*, 100(5), pp. 54502(1)-54502(4).
 14. ROSTAMZADEH, N., KELSO, R. M. and DALLY, B. (2017) 'A numerical investigation into the effects of Reynolds number on the flow mechanism induced by a tubercled leading edge', *Theoretical and Computational Fluid Dynamics*, 31(1), pp. 1-32.
 15. SKILLEN, A., REVELL, A., PINELLI, A., PIOMELLI, U., and FAVIER, J. (2015) 'Flow over a wing with leading-edge undulations', *AIAA Journal*, 53(2), pp. 464-472.
 16. SRINIVAS, K. S., DATTA, A., BHATTACHARYA, A., KUMAR, S. (2018) 'Free-stream characteristics of bio-inspired marine rudders with different leading-edge configurations', *Ocean Engineering* 170, pp. 148-159.
 17. STERN, F., WILSON, R. V., COLEMAN, H. W., PATERSON, E. G. (1999) 'Verification and Validation of CFD Simulations', IOWA INST OF HYDRAULIC RESEARCH, IIHR Report No. 407
 18. WEI, Z., TOH, J. W. A., IBRAHIM, I. H., and ZHANG, Y. (2019) 'Aerodynamic characteristics and surface flow structures of moderate aspect-ratio leading-edge tubercled wings', *European Journal of Mechanics-B/Fluids*, 75, pp 143-152.

